Requirements for efficient metal oxide photocatalysts for CO_2 reduction

10

Jennifer Strunk
Leibniz Institute for Catalysis at the University of Rostock, Rostock, Germany

10.1 Introduction

Within the current discussion concerning changing raw material and energy supply, there is no doubt that one molecule around us is present in large excess: carbon dioxide. Although still fairly diluted in air, the CO_2 concentration has not dropped below 400 ppm in the year 2016, which marks a record high [1]. As product of any combustion process of organic molecules, CO_2 is widely produced as by-product in the energy, transport, and production sectors. For example, for a regular passenger vehicle with a fuel consumption of ~7 L per 100 km, a quick estimation of carbon emissions yields an amount of approximately 150 g CO_2 emitted for each single kilometer. It is now widely accepted that CO_2 is one of the main contributors to global warming. Although CO_2 is continuously removed from air by the natural carbon cycle, consisting of photosynthesis in plants as well as inorganic processes, the natural carbon cycle cannot keep up with humankind's enormous CO_2 emissions. Recycling carbon dioxide to fuel (additives) or raw materials for the chemical industry using just the energy of sunlight would be the ideal way to address both the reduction of carbon emissions and the supply of renewable resources for energy and production [2,3]. This is not a new idea: A few chemical processes have already used CO_2 as reactant for decades, for example for the synthesis of urea, salicylic acid, and cyclic organic carbonates [4]. It is also well known that in the industrial methanol synthesis over Cu/ZnO catalysts, CO_2 rather than CO is the primary carbon reactant in the synthesis gas feed [5–7], and modern research initiatives aim at making methanol solely from CO_2 and regeneratively produced H_2 [5]. However, industrial processes such as methanol synthesis currently rely on fossil fuels and traditional synthesis gas generation, so they do not contribute to CO_2 recycling. Thus, other ways have to be found to convert CO_2 without using fossil fuels, and without producing additional carbon emissions.

The first attempts to activate and react CO_2 photoelectrochemically or photocatalytically already date back to the late 1970s and the pioneering works of Halmann [8] and Inoue et al. [9]. Regardless, during the past almost 40 years, significant progress that would make such a process viable on the industrial scale has not yet been achieved [2]. Due to the high thermodynamic and kinetic stability of the CO_2 molecule [4], only extremely low yields have been obtained in previous studies.

Metal Oxides in Energy Technologies. https://doi.org/10.1016/B978-0-12-811167-3.00010-9

A compilation by Kondratenko et al. [5] revealed that in most studies reported between the 1980s and 2013s, the yields of the product methane by photocatalytic processes did not exceed 10 μmol g^{-1} h^{-1}. This has also been discussed in the review by Habisreutinger et al. [2]. This is far below a productivity that would attract the attention of the chemical industry. Apart from the main challenge to increase product yields, current photocatalysts that can convert CO_2 also face low selectivity, in which a variety of products such as carbon monoxide, methane, methanol, formic acid, and even longer hydrocarbon chains are often obtained in the same process.

In this chapter, the materials commonly studied in photocatalytic CO_2 reduction are discussed, revealing that the vast majority of them are based on oxides. In the following parts of the chapter, the principles of photocatalysis in general and of photocatalytic CO_2 reduction in particular are briefly explained. Possible adsorption modes of CO_2 on oxides and suggested mechanisms of photocatalytic CO_2 reduction are then discussed, with a particular focus on titanium dioxide-based materials. This is then followed by some remarks on photoreactors and reaction conditions that are important for reliable studies of oxide-based and other materials in photocatalytic CO_2 reduction. In the final sections of this chapter, the current state of the art of photocatalytic CO_2 reduction using some commonly used oxide materials is described.

10.2 Overview of photocatalysts for CO_2 reduction

To obtain an overview of photocatalyst materials studied for CO_2 reduction in the past, a structured literature search was performed, considering all original research papers on photocatalytic CO_2 reduction written in English that were published until the end of November 2014. Conference contributions and review papers were neglected. Only purely inorganic heterogeneous photocatalysts were considered. Anchored or tethered complexes with a ligand sphere on solid surfaces, as well as photocatalysts with major organic components (e.g., metal–organic frameworks, dye-sensitized systems) were neglected. Pure TiO_2 was not counted in a specific publication when it was only used as a reference material.

In total, 277 papers were considered, in which 443 photocatalysts were studied. The tested photocatalyst systems can be grouped into ten material classes:

- *Bulk TiO_2 based*, for example, pure crystalline phases, TiO_2 with (noble) metal cocatalysts, bulk- and surface-doped TiO_2 (total: 48%);
- *Pure* (simple) *oxides* other than TiO_2 (e.g., MgO, ZrO_2, ZnO, Cu_xO) (total: 6%);
- *Complex oxides*, such as mixed oxides, perovskite and pyrochlore structures, for example, titanates, niobates, or tungstates (total 14%);
- Systems based on *isolated titanate* species with tetrahedral TiO_4 geometry (total 7%; more than three quarters of all publications by Masakazu Anpo's group);
- *Nonisolated TiO_2/SiO_2* systems, that is, where TiO_x species were supported on or mixed with silica, but are not present as isolated photoactive TiO_4 species (total 5%);
- Pure *sulfides*, for example, CdS, ZnS, and Bi_2S_3 (total 4%);
- *Carbon-based materials*, for example, C_3N_4, graphene oxide, and carbon nanoparticles (total 3%);

- *Layered double hydroxides* (LDHs, total 2%);
- *Other semiconductors*, for example, GaN and SiC (total 2%);
- *Other isolated metal cations* or bimetallic purely inorganic complexes functioning as photoactive species, for example, Zn-Ti/SiO_2, Cr-Ti/SiO_2, and Zr-O-Co/SiO_2 (total 1%).

The remaining 9% of systems consists of mixed materials (e.g., mixtures of pure oxides, semiconductors supported on complex oxides, etc.; total: 5%) and miscellaneous materials, not belonging to any category (e.g., Ag@AgBr/CNT, NiO_x-Ta_2O_5/graphene, etc.; total: 4%). The percentage of systems studied in each category is visualized in Fig. 10.1.

It becomes evident that almost half of all studied systems were based on any of the forms of pure TiO_2 (48%). Non-TiO_2 oxides and complex oxides comprise another 20% of all studied systems. A further 13% are made up of isolated photoactive TiO_4 species or bulk TiO_2 in a silica matrix, so those systems are also purely oxide materials. The mixed systems, contributing 5% of all studied systems, also contain at least one oxide component. Thus, in summary, 86% of all photocatalyst systems studied until November 2014 for photocatalytic CO_2 reduction were oxide based.

Over recent 2 years (2015 and 2016), research has diverged into a variety of different directions, in which particularly mixed systems and complex composites of multiple materials have been studied, partially in the form of *Z*-scheme systems. It is thus almost impossible to define material classes. However, a few materials stand out and were studied more frequently, either by themselves or in composites, particularly carbon-based materials, such as graphitic carbon nitride [10–23], graphene, and others [11,12,24–34]. Returning the focus on oxides, materials such as In_2O_3 (as oxide or dopant) [35–43], copper oxides [27–30,44–47], sodium tantalates [48,49],

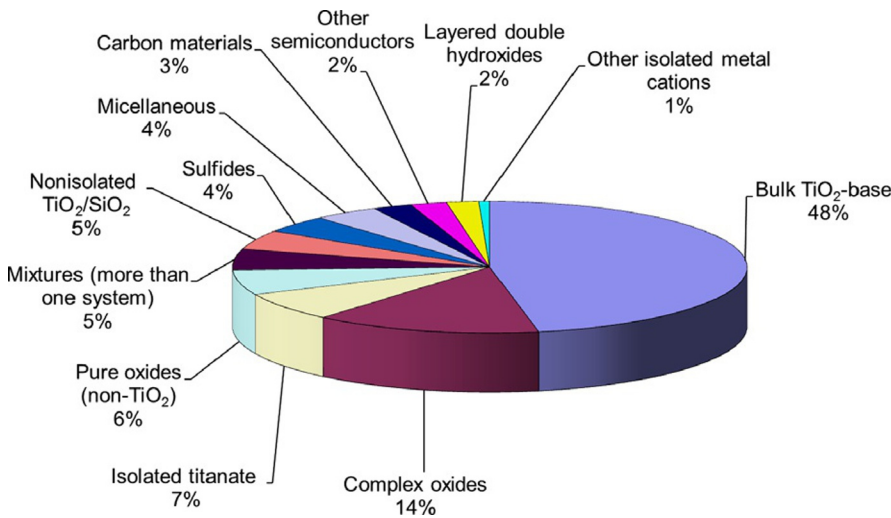

Fig. 10.1 Overview of heterogeneous photocatalyst systems studied for photocatalytic CO_2 reduction until November 2014; specific criteria of literature search: see text.

strontium titanates [47,50,51], and LDH-derived structures [52–58] were frequently applied, either pure or in composites. Furthermore, (nanostructure-engineered and doped) TiO_2 continues to be an interesting and frequently studied material [32–38,44,53,59–75]. Some insight into the different material classes listed above will be given near the end of this chapter. It needs to be noted early on, however, that only for TiO_2 and related materials (e.g., the isolated titanate), some progress toward understanding of the mode of action could be achieved so far [2]. Still, none of the studies on TiO_2-related materials has yet shown significant (i.e., order of magnitude) improvements in yields. Studies of all other systems are mostly standing on themselves, and the potential of these systems appears underexplored. Before the behavior of some of the materials listed above in photocatalytic CO_2 reduction is considered, it is useful first to take a look at the general principles of photocatalytic processes.

10.3 Basics of heterogeneous photocatalysis

A material that is to be used as heterogeneous photocatalyst needs to fulfill a number of functions. Light needs to be absorbed, ideally in the visible region, and charge carriers need to be generated, separated, and migrate to the surface of the material. Apart from those suitable photophysical properties the material needs to feature suitable catalytic properties. Active sites need to be present on the surface where reactants can bind and react with the photogenerated charges to the desired products, ideally with high reaction rates and low activation energy [2]. If a certain material does not feature efficient catalytic active sites on the surface, it is possible to add a cocatalyst [2], which facilitates either the oxidation reaction (hole transfer from semiconductor to reactant) or the reduction reaction (electron transfer from semiconductor to reactant). In the following, the requirements listed above will be briefly introduced. They are also visualized in Fig. 10.2. For a more detailed discussion, the reader is referred to previous excellent publications [2,3,76–81].

The processes occurring upon photoexcitation in a semiconductor can be considered from different perspectives (Fig. 10.2). The spatial view looks at the migration of the charge carriers and their further reactions, such as recombination or redox reactions (Fig. 10.2, left). The energetic view considers the processes occurring within the band structure of the semiconductor (Fig. 10.2, top right). Lastly, the processes occurring at the surface, such as the electron transfer onto an adsorbed acceptor molecule need to be considered (Fig. 10.2, bottom right). All those processes are discussed below.

For a semiconductor, the light energy that can be absorbed by the material is related to its bandgap. The band structure in semiconductors arises from the overlap of near infinite electronic states of the constituent atoms. Those electronic states fully occupied by electrons in the ground state at $T = 0\,K$ form the valence band, and the unoccupied states form the conduction band. In between, a gap exists in which no electronic states are available, which is referred to as the bandgap [2,76,82]. Photoexcitation with light of photon energy larger than the bandgap excites an electron from the valence band to an excited state in the conduction band (Fig. 10.2, top right).

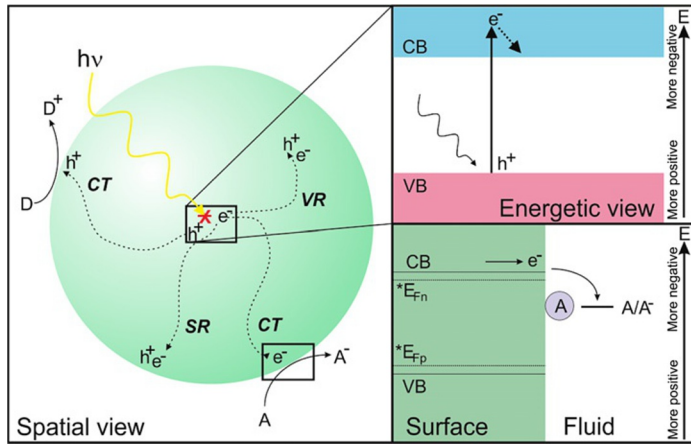

Fig. 10.2 Schematic representation of the processes occurring in heterogeneous photocatalysis. *Left*: Spatial view of charge carrier generation (e^-, h^+) upon irradiation with light of suitable energy, with *VR* = volume recombination, *SR* = surface recombination, *CT* = charge transfer processes. *Top right*: Energetic view of the excitation of an electron from the valence band (VB) to the conduction band (CB) and relaxation processes to the bottom of the conduction band. *Bottom right*: Processes occurring at the surface of a photocatalytic nanomaterial under irradiation, including the formation of quasi-Fermi levels and the transfer of an electron onto an adsorbed acceptor molecule A with a reduction potential less negative than the CB minimum. Based on A.L. Linsebigler, G. Lu, J.T. Yates, Chem. Rev. 95 (1995) 735 (left part) and R. Beránek, Adv. Phys. Chem. (2011) 786759 (bottom right).

Regardless of the exact energy state within the conduction band in which the electron will end up, it will relax practically immediately to the bottom of the conduction band [2,76,83]. The loss of an electron leaves behind an empty state at the top of the valence band, referred to as a hole (h^+). Consequently, the most relevant electronic states for photocatalysis are those at the top of the valence band and the bottom of the conduction band (Fig. 10.2, top right). In TiO_2, the top of the valence band is made up by the oxygen 2p states, while the lowest unoccupied states forming the bottom of the conduction band are Ti 3d states [78,84]. Semiconductors are often classified in two groups, those with a direct bandgap (e.g., TiO_2 rutile) and those with an indirect one (e.g., TiO_2 anatase). When optical transition (excitation and recombination) does not require a change in momentum, the transition is termed as being direct. For indirect optical transitions, both a photon and a phonon need to be involved. For more information, the reader is referred to Refs. [79,85,86].

In semiconductors, the charge carriers generated upon photoexcitation can migrate rather freely through the solid. It is desired that they reach the surface to participate in charge transfer reactions (Fig. 10.2, left, *CT* = charge transfer). However, charge carriers are lost due to recombination phenomena of a photoexcited electron and a hole, which can happen both on the surface (Fig. 10.2, left, *SR* = surface recombination) and in the bulk of the semiconductor (Fig. 10.2, left, *VR* = volume recombination).

This lowers the achievable efficiency of the photocatalytic reaction [2]; therefore, the recombination rate should be as low as possible. Recombination events are influenced by the mobility of charges and by charge trapping. Defects within the semiconductor lattice or an interface with another material that traps one type of the charges (electron or hole sink) can act as recombination sites [2]. Conversely, interfaces between different semiconductors [3] or a semiconductor and a metal [2,3] may also be favorable to separate charges. The term "diffusion length," a material-dependent quantity, is defined as the average distance that a charge carrier can migrate before recombination takes place [2]. In this respect, it may be beneficial to use nanomaterials for photocatalysis: if the particle size is smaller, then the distance that the charge carriers need to migrate before they reach the surface is shorter and the ratio with respect to the diffusion length is more favorable [87].

It is not only the size of the bandgap that determines whether a material can be used for a specific photocatalytic process. The energy levels also need to be properly positioned so that both the reduction and the oxidation reaction are thermodynamically allowed. The thermodynamically spontaneous process for electrons is to fall down to lower energy levels, so a reduction reaction on the surface of a semiconductor is only possible if the excited electron at the bottom of the conduction band is situated at a higher energy compared to the acceptor level of the molecule to be reduced. In other words, the conduction band minimum needs to be at a more negative potential on the electrochemical energy scale than the reduction potential of the acceptor molecule (Fig. 10.2, bottom right). Conversely, if an electron in a donor molecule is supposed to fill up a hole in the valence band, thereby oxidizing the donor, then the valence band maximum needs to be situated at a more positive potential than the oxidation potential of the donor [2,76,88]. This is often summed up in the statement that the band edges of the semiconductor need to straddle the redox potentials of the desired reactions [85]. It is often not sufficient that the potential of the conduction band minimum is just above (more negative than) the potential of the reduction reaction, and that the valence band maximum is just more positive than the oxidation reaction. Kinetic barriers of the reaction require providing an overpotential on each side so that the reaction can run with high rate [2]. The better the catalytic function of the photocatalyst, the lower will be the kinetic barrier and thus the required overpotential, but without any overpotential high rates are not achievable even with good catalysts [2]. It should be kept in mind that taking the conduction band minimum and valence band maximum as decisive factors for thermodynamic feasibility is a simplification, since precisely the quasi-Fermi levels of electrons ($^*E_{Fn}$) and holes ($^*E_{Fp}$) in the semiconductor need to be considered [2,84] (Fig. 10.2, bottom right). However, taking the position of the band edges is a reasonable approximation, particularly for TiO_2 and other n-type semiconductors [2,84].

Apart from existing sufficiently long and reaching the material's surface, the charges generated must be used for specific chemical reactions, ideally with a high rate. Consequently, the material needs to feature appropriate catalytic active sites on the surface that adsorb the reactants and stabilize relevant reaction intermediates. This condition is similar to classical (thermal) heterogeneous catalysis: by adsorption of at least one of the reactants on its surface, the heterogeneous catalyst offers an

energetically more favorable reaction pathway and lowers the activation barrier of the process. Knowledge-guided design of the catalytic functionality of a photocatalyst for carbon dioxide reduction is currently still hindered by the fact that the preferred reaction pathway is not yet fully clear. Possible adsorbates and reaction intermediates are discussed in detail below, together with possible reaction mechanisms.

The principles outlined above refer to semiconductors as photocatalysts. However, another important class of oxide-based heterogeneous photocatalysts for CO_2 reduction consists of isolated photoactive (transition) metal cations on or in an inert oxide-based matrix, usually silica. For an isolated photoactive species, photoexcitation promotes an electron from the highest occupied molecular orbital (HOMO) to the excited state in the lowest unoccupied molecular orbital (LUMO). The necessary energy for this process is determined by the gap between HOMO and LUMO. For an isolated tetrahedral TiO_4 (titanate) species (Fig. 10.3, right), photoexcitation can be understood in terms of a ligand-to-metal charge transfer, in which an electron is transferred from one of the oxygen ligands to the central Ti cation [89] (Eq. 10.1):

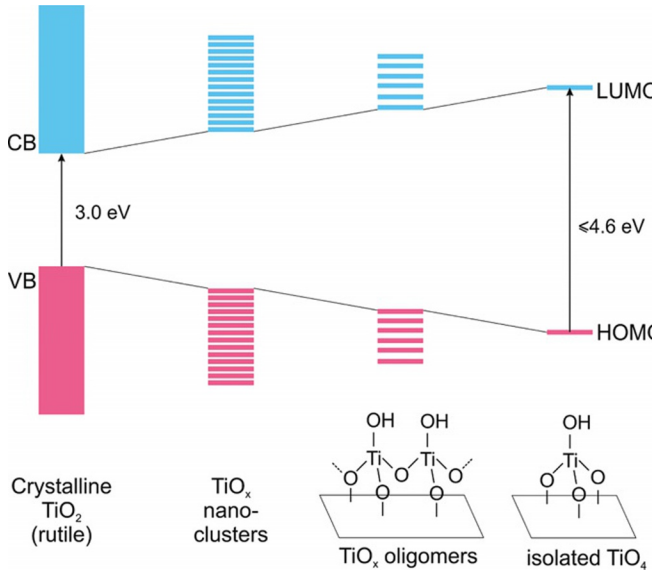

Fig. 10.3 Schematic representation of the quantum size effect; development of electronic states when going from the semiconductor TiO_2 (thermodynamically stable rutile phase with direct bandgap) over nanoclusters to TiO_2 oligomers and to the isolated titanate species on inert supports.
Modified from M. Matsuoka, M. Anpo, Local structures, excited states, and photocatalytic reactivities of "single-site" Ti-oxide photocatalysts constructed within zeolites or mesoporous materials, in: M. Anpo, P.V. Kamat (Eds.), Environmentally Benign Photocatalysts: Applications of Titanium Oxide Based Materials, Springer Science-Business Media, New York, 2010; D.W. Bahnemann, C. Kormann, M.R. Hoffmann, J. Phys. Chem. 91 (1987) 3789.

$$\left[Ti^{4+} - O^{2-}\right] \; h\nu \; h\nu \; \left[Ti^{3+} - O^{-}\right] \tag{10.1}$$

If the photoactive species is supported on an insulating support, neither type of charge carrier can be transported away. Instead, both electron and hole are localized at the photoactive species, requiring that the same species also needs to be the active catalyst. Only if conducting supports are used, or if noble metals are brought in close proximity, then electrons may be transferred to or from the photoactive species.

If materials based on the same transition metal cation are considered—most importantly bulk TiO_2 and the isolated tetrahedral titanate (TiO_4) species—then the bandgap excitation in the semiconductor always requires less energy than the corresponding HOMO-LUMO excitation in the isolated photoactive species (Fig. 10.3). This is a consequence of the interacting electronic states from neighboring atoms in a crystal lattice, leading to the formation of wide bands in extended semiconductors [82]. Since both the occupied states (the valence band) and the unoccupied states (the conduction band) develop into a broad and practically continuous band of energy states, the gap between them is narrower than the gap between a single HOMO and LUMO of an isolated species. Once the dimensions of a semiconductor become small enough, it becomes noticeable that less and less electronic states overlap, so that the band structure transforms more and more into an assortment of discrete electronic levels. This is then reflected in an increase of the energy required for photoexcitation [80,90], an observation commonly referred to as the *quantum size effect* [76,89] (Fig. 10.3). Considering the thermodynamic requirements that the excited electron should always be at a more negative potential than that of the reduction reaction to be carried out, and the hole at a more positive potential than the oxidation reaction, the benefit of using isolated tetrahedral titanate sites as compared to bulk TiO_2 can be easily rationalized with the more negative and positive potentials of the electron in the LUMO and the hole in the HOMO compared to photogenerated charge carriers in the conduction band and the valence band of crystalline TiO_2, respectively.

Many publications highlight nanosize and nanostructuring of oxides as possible means for the photocatalyst improvement [91–99]. Looking at this from a physical and chemical point of view, nanostructuring of the photocatalyst is beneficial for two reasons: firstly, the distance that the charges need to migrate before they reach the surface is shorter, which is favorable with respect to the carrier diffusion length. Secondly, nanostructured materials have a high surface-to-volume ratio, so that they may offer more catalytic active sites on the surface [2,80,87,91]. However, it should also be considered that catalytic active sites do not necessarily scale simply with the total surface area. An example is pure zinc oxide as (thermal) heterogeneous catalyst in methanol synthesis, where a simple increase in surface area does not increase catalytic activity further, since well-developed polar surfaces are required to expose catalytically highly active sites, such as oxygen vacancies [100–102]. It has also been suggested that the presence of polar surfaces on ZnO is beneficial for its activity in photocatalytic dye degradation reactions [103]. Furthermore, when nanostructured materials are used in photocatalysis, it must also be considered that a larger amount of defects is likely to be present in the material, and that interparticle charge transfer

may be slowed down. For a detailed discussion of the effect of nanostructuring, the reader is referred to Ref. [97]. In any material, defects can be grouped into *point defects*, which are discussed below; *linear defects*, for example, dislocations; *planar defects*, in particular surfaces and grain boundaries; and *spatial defects*, such as small nanoparticles in a host phase. The large group of *point defects* in oxides comprises cation vacancies, oxygen vacancies, interstitial cations, electronic defects, and foreign ions in lattice or interstitial sites. Interstitial oxygen, on the other hand, is extremely rare. To satisfy the condition of charge neutrality of the crystal, charges added to or removed from the crystal must be internally compensated for [79]. While all defects will affect charge carrier lifetime, that is, charge migration and recombination rates, it is particularly relevant to consider oxygen vacancies as defects in oxides: TiO_2 is a native n-type semiconductor due to a natural occurrence of oxygen vacancies. This is related to the presence of Ti^{3+} cations [79,81], because the formation of oxygen vacancies by removal of oxygen from the lattice is accompanied by the transfer of two electrons to the neighboring titanium cations, reducing them from the +4 to the +3 oxidation state [104–106]. In ZnO, an "empty" V_O^{2+} vacancy may trap either one electron (V_O^+) or two electrons (V_O^0) [107]. While it was believed for a long time that oxygen vacancies are also the source of intrinsic n-type semiconducting behavior of ZnO, recent density functional theory calculations and electron paramagnetic resonance investigations came to the conclusion that this assignment cannot be correct. Instead, the n-type conductivity may be related to unintentional doping, for example with interstitial hydrogen [108]. While the topic of defects in oxides is certainly relevant for considerations of photocatalytic activity, a detailed discussion is outside the scope of this chapter. Instead, it will just be pointed out that for the case of TiO_2 (and Cu/TiO_2), the presence of oxygen vacancies, in particular on the brookite polymorph, has been suggested by the group of Ying Li to be beneficial for its activity in photocatalytic CO_2 reduction [109,110]. On the basis of high-level computational results, such as excited-state ab initio calculations of CO_2 adsorbed on clusters from the (010), (101), and (001) anatase surface planes, Indrakanti et al. [111] even came to the conclusion that on TiO_2 electron transfer to CO_2 is possible solely in the presence of oxygen vacancies. Only then, a strongly bound, bent adsorbate species can be formed from CO_2, and electron transfer becomes possible. While this is certainly an important piece of information, it should be kept in mind that oxygen vacancies or Ti^{3+} may also participate in stoichiometric reactions [111] in which CO_2 is reduced and/or oxygen atoms are removed from CO_2, so to put forward such a hypothesis requires careful evaluation of the catalytic nature of the overall process.

10.4 Involved (elementary) reactions and energetic requirements of CO_2 reduction

It has recently been suggested that photocatalysts for CO_2 reduction could only be improved substantially if an in-depth understanding of the reaction mechanism is achieved. However, such a level of understanding has not been reached [2]. Different reaction pathways may be in operation dependent on the reaction conditions and

employed catalysts, and some fundamental questions concerning the elementary step mechanism have not yet been solved.

In the carbon dioxide molecule, the carbon atom is in the +4 oxidation state. For the formation of methane, it needs to be reduced by a total of eight electrons to reach the oxidation state −4. Not only is this an eight-electron reaction, but it also requires the removal of both oxygen atoms from the molecule. Formation of methane is not the only possible reaction. The C_1 reaction products observed in photocatalytic CO_2 reduction also comprise carbon monoxide and formic acid (two-electron processes), formaldehyde (four-electron process), and methanol (six-electron process). Products containing two or more carbon atoms have also been observed, such as ethane, ethylene, ethanol, oxalic acid, acetaldehyde, or higher hydrocarbons and alcohols [2]. The ideal reducing agent and proton source for the formation of hydrocarbons and oxygenates from CO_2 would be plain water [112], but then also the water splitting reaction needs to proceed concomitantly. In any case, reaction stoichiometry requires the formation of products from the surplus oxygen anions and holes, ideally gaseous O_2, but another potential product would be hydrogen peroxide [2].

Since CO_2 and H_2O are thermodynamically extremely stable, forming any C- and H-containing products from those two molecules is always an endergonic reaction ($\Delta G > 0$), that is, the reaction needs to proceed thermodynamically uphill [2,112]. It has become common practice to refer to this reaction as being "photocatalytic," but the correct term would be "photosynthetic" [2]. (Heterogeneous) Catalysts, by definition, can only accelerate reactions that are anyhow thermodynamically downhill ($\Delta G < 0$) [113], since they only lower the activation energy by offering an energetically more favorable reaction pathway on their surface. The possibility to carry out a photosynthetic (endergonic) reaction with a photocatalyst originates from the fact that the energy is provided by the incident photons [2] by the generation of an excited state, and the fact that the oxidation and reduction reaction are spatially separated [113]. This is the reason for the thermodynamic requirement outlined above, stating that the conduction band minimum of the semiconductor always needs to be at a more negative potential compared to the reduction potential of the acceptor molecule, while at the same time the valence band maximum must be at a more positive potential than the oxidation potential of the donor molecule. Only if this condition is fulfilled, the separate half reactions, reduction of the acceptor and oxidation of the donor, are thermodynamically allowed [113].

As mentioned above, reaction stoichiometry requires that both photogenerated electrons and holes are consumed, and that oxygen (or hydrogen peroxide) is formed as by-product from an oxidation reaction of one or both oxygen anions originating from the CO_2 molecule and/or the secondary reactant H_2O. The following Eqs. (10.2)–(10.4) exemplify the formation of methane in an eight-electron process. Overall reaction:

$$CO_2 + 2\,H_2O \xrightarrow{h\nu,\ cat} \xrightarrow{h\nu,\text{cat}} CH_4 + 2\,O_2 \qquad (10.2)$$

Reduction:

$$CO_2 + 8\,H^+ + 8\,e^- \rightarrow CH_4 + 2\,H_2O \tag{10.3}$$

Oxidation:

$$2\,H_2O \rightarrow O_2 + 4\,H^+ + 4\,e^- \tag{10.4}$$

However, with few exceptions (e.g., Refs. [46,109,114,115]), the formation of oxygen is usually not reported in the literature, either because it was not studied at all, or because oxygen was not formed. This challenge of oxygen evolution is related to photocatalytic or photoelectrochemical water splitting [116], where this step, involving four holes per oxygen molecule, is thought to be the more demanding step in the overall process [2], associated with high kinetic barriers, or, in other words, with high overpotentials [117]. Apart from the difficulty to form the oxygen, it may also not desorb and remain on the surface of the photocatalyst. Alternatively, other products may be formed instead of gaseous dioxygen, such as hydroxyl or superoxide radicals. Due to their high reactivity, those species might oxidize products or intermediates of photocatalytic CO_2 reduction [2] and thereby strongly limit achievable yields. In this respect, the rapid degradation of hydrocarbons on photocatalysts for CO_2 reduction has been demonstrated previously [118]. Highly efficient catalysts for oxygen evolution, for example iridium or ruthenium oxide, are extremely rare and expensive, again strongly limiting the potential for large-scale application. All in all, it should be stated that the oxidation reaction is the much less studied process in photocatalytic CO_2 reduction [2,119], so that the fate of the holes and the surplus oxygen atoms is still virtually unknown.

The one-electron reduction of CO_2 to the anion radical $CO_2^{-}\cdot$ requires a potential of $-1.9\,eV$ and is therefore an extremely challenging reaction. This is due to the high chemical stability and extremely low electron affinity of the CO_2 molecule [2,3]. Electron addition requires breaking molecular symmetry. The formerly linear CO_2 molecule bends after taking up an electron due to repulsion of the additional electron located at the carbon atom and the free electron pairs of the oxygen atoms. Since such processes are energetically highly unfavorable, the LUMO of the CO_2 molecule is located at very high energy [4]. The conduction band of virtually no semiconductor is appropriately positioned to allow this reaction without any applied bias [2].

So, in a pure photocatalytic process in the presence of a gas phase above a semiconductor, this elementary step is not expected to occur. However, it should be considered that adsorption processes of CO_2 on the semiconductor surface may already bend and partially charge the CO_2 molecule, thus destabilizing it. This lowers the LUMO and makes electron transfer reactions slightly more favorable [2,4]. Alternatively, instead of a single electron transfer, proton-assisted transfers of multiple electrons may occur. With respect to the required potential, they are more easily achieved from a thermodynamic viewpoint [2,3]. However, it appears unreasonable to assume that such complicated processes involving multiple charge carriers and many reaction

Table 10.1 Some reactions potentially related to photocatalytic CO_2 reduction, hydrogen and oxygen evolution together with their redox potentials at pH = 7 in aqueous solution.

Reaction	E^0 (V vs NHE)
$2\ H_2O \longrightarrow O_2 + 4H^+ + 4e^-$	+0.81
$2H^+ + 2e^- \longrightarrow H_2$	−0.42
$CO_2 + e^- \longrightarrow CO_2^{\bullet -}$	−1.90
$CO_2 + 2H^+ + 2e^- \longrightarrow HCOOH$	−0.61
$CO_2 + 2H^+ + 2e^- \longrightarrow CO + H_2O$	−0.53
$CO_2 + 4H^+ + 4e^- \longrightarrow H_2CO + H_2O$	−0.48
$CO_2 + 6H^+ + 6e^- \longrightarrow CH_3OH + H_2O$	−0.38
$CO_2 + 8H^+ + 8e^- \longrightarrow CH_4 + 2H_2O$	−0.24

(Values of standard potentials taken from L. Guo, Y. Wang, T. He, Chem. Rec. 16 (2016) 1918.)

partners are elementary steps, especially because hardly any evidence for such concerted reactions has so far been obtained [2]. Table 10.1 presents an overview of reactions that have been suggested to be potentially related to photocatalytic reduction of CO_2 and evolution of H_2 and O_2, together with their redox potentials at pH = 7 [3].

Studies of reaction mechanisms in photocatalysis in general and in CO_2 reduction in particular are vastly complicated by the fact that reaction intermediates are often radical species with high reactivity and short lifetime. The high reactivity implies numerous possibilities in which they can reach further, leading to strongly branched and complex reaction networks [2]. The short lifetimes make it difficult to detect all relevant intermediates.

Already the first stages of any reaction mechanism of photocatalytic CO_2 reduction are a matter of debate. In general, additional to simply linearly physisorbed CO_2, (reactive) adsorption of CO_2 on oxide surfaces can generate a variety of adsorbed surface species, namely carbonates, bicarbonates, carboxylates, and formate species. A very thorough discussion of CO_2 adsorption on oxides has been provided by Busca and Lorenzelli [120]. The possible structures that can be formed on oxide surfaces are visualized in Fig. 10.4 together with the original enumeration from Ref. [120].

Another possible surface intermediate is the carboxyl species (not shown in Fig. 10.4), an actual organic acid functional group (*COOH; asterisk indicates an adsorbed species). Regarding the composition, carboxyl species are similar to formates (*HCOO), but in carboxyl species the hydrogen atom is attached to an oxygen atom instead of the central carbon atom. It should also be noted that on zinc oxide an unusual tridentate carbonate species has been detected previously [121].

While carbonate species are formed whenever a surface (lattice) oxygen atom is involved in CO_2 adsorption, bicarbonates can be formed from a reaction of CO_2 with a surface hydroxyl group. The formation of formates requires some activated form of hydrogen. The different adsorbates can be distinguished by vibrational spectroscopy, as it has been discussed in detail in Ref. [120]. For TiO_2 in photocatalytic CO_2 reduction, enhancing the formation of (bi)carbonates on the surface by addition of sodium cations has recently been shown to be detrimental for

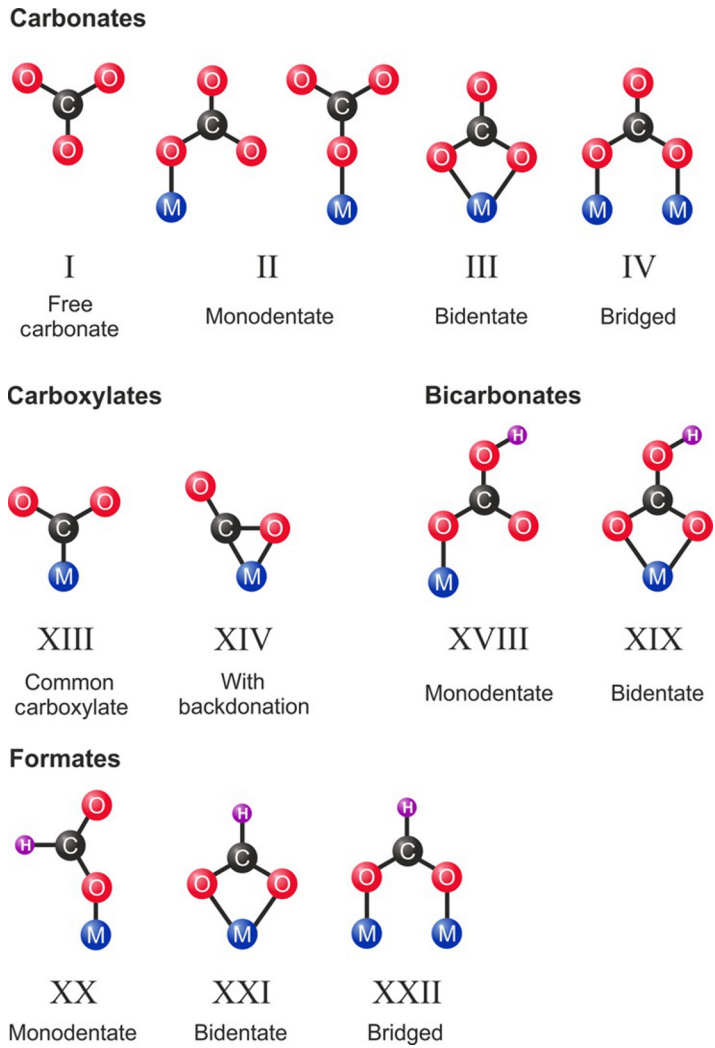

Fig. 10.4 Possible structures of adsorbates formed upon CO_2 adsorption on oxide surfaces together with the original classification and enumeration by Busca and Lorenzelli [120].

methane production [59]. Furthermore, for Cu/TiO_2, where the participation of carbonaceous impurities on the surface in photocatalytic CO_2 reduction was clearly demonstrated, it was still found that surface carbonates decompose mostly to CO_2 under illumination [122]. It is thus possible that the formation of (bi)carbonate on the surface is detrimental rather than beneficial, either because those species are too stable for any further reaction, or because they act as hole traps rather than attracting electrons needed for a reduction reaction [2,123]. On the other hand, for a doping of TiO_2 with bismuth it has been found that a stronger adsorption of CO_2 was beneficial to increase the yields of methane [62]. An enhanced

adsorption of CO_2 was also discussed as one reason for the improved activity of TiO_2 coated with a thin silica shell, although the presence of Ti—O—Si bonds was also suggested to play a role in causing an improved charge carrier lifetime [73]. In contrast to this finding, acidification of the TiO_2 surface by treatment with sulfuric acid increased methane yields as well. In those nanosheet samples, with predominantly exposed {001} and {101} facets, the improvement caused by acid treatment was attributed to the formation of surface hydroxyl groups and oxygen vacancies/Ti^{3+} species. This then increased charge carrier lifetime [66].

So far, actual reaction mechanisms were only discussed for TiO_2, because for this material the most detailed studies have been performed. Currently (2016), the mechanistic steps are not unambiguously clear, but three main routes have been discussed in the literature [2,124–126], which are visualized in Fig. 10.5 and are discussed below.

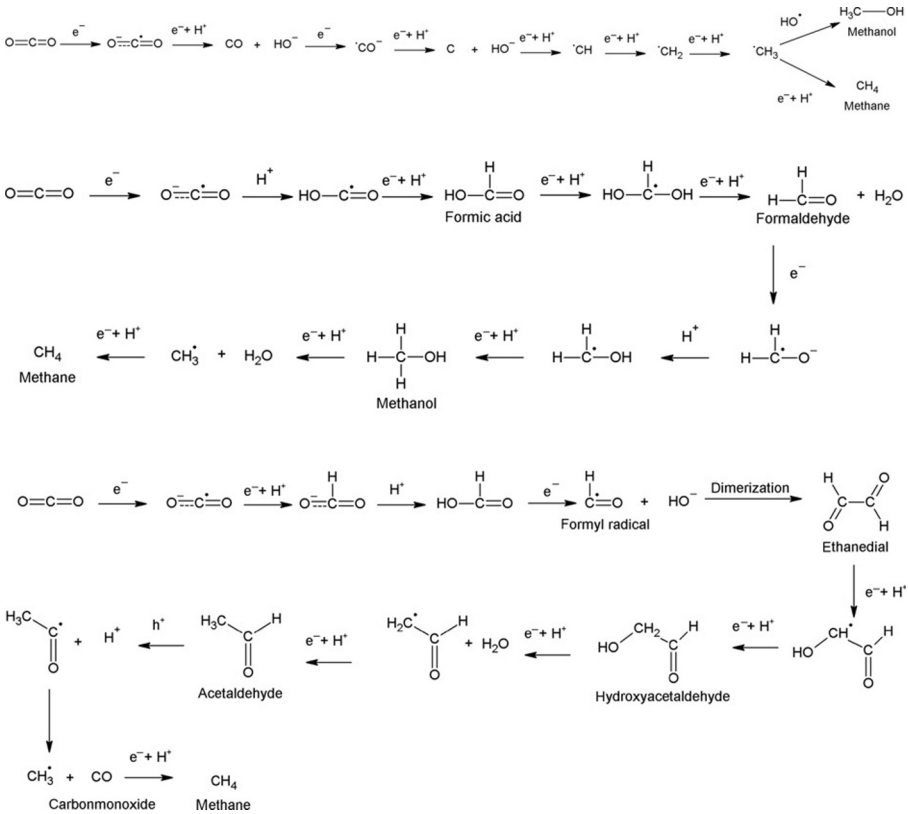

Fig. 10.5 Schematic representation of three proposed pathways of photocatalytic CO_2 reduction.
Modified from S. Cao, J. Low, J. Yu, M. Jaroniec, Adv. Mater. 27 (2015) 2150; K.A.S. Fernando, S. Sahu, Y. Liu, W.K. Lewis, E.A. Guliants, A. Jafariyan, P. Wang, C.E. Bunker, Y.-P. Sun, ACS Appl. Mater. Interfaces. 7 (2015) 8363.

Following the nomenclature in Ref. [2], all three mechanisms are named after a unique intermediate, being referred to as *formaldehyde pathway*, *carbene pathway*, and *glyoxal pathway*. It must be noted that the observation of different intermediates and thus reaction mechanisms may be related to the considerably varying reaction conditions applied in previous studies, in particular with respect to light intensity, liquid- or gas-phase reactor operation, or the concentration of CO_2, H_2O, and potential other additives. In the following discussion, the different mechanisms will be briefly described.

10.4.1 Carbene pathway

This mechanism has been supported already in very early studies by the group of M. Anpo for isolated titanate species on silica as photocatalysts, in particular based on EPR detection of C, H, and CH_3 radicals [127,128]. The anion radical $CO_2^{-}\cdot$ is initially split to yield CO and a hydroxyl species. With the assistance of another proton and electron transfer, the second oxygen atom is also removed as hydroxyl species, and carbon atoms are obtained. These are successively hydrogenated by hydrogen radicals until a methyl radical (CH_3) is obtained. This can be hydrogenated to yield methane, or it can undergo a reaction with a hydroxyl radical to yield methanol. So, different from the formaldehyde mechanism, methanol and methane are not formed consecutively, but in parallel reactions.

10.4.2 Formaldehyde pathway

This mechanism starts from the anion radical $CO_2^{-}\cdot$, from which a carboxylate (COOH) and then formic acid is formed. A dihydroxymethyl [$HC(OH)_2$] radical formed by another H radical addition then dehydrates to the key intermediate formaldehyde (H_2CO). Another electron and proton transfer leads to the formation of hydroxymethylene (H_2COH), from which methanol is consecutively formed. The further reduction of the methanol leads to the formation of methyl radicals (CH_3) with release of water, and finally the formation of methane [2]. This mechanism has been described as the "simplest" reaction scheme, because it can be considered a sequence of four consecutive two-electron proton-coupled reactions [125]. It should be noted that although the formaldehyde pathway has been discussed in detail in Ref. [125], the same article provides convincing evidence against this reaction pathway.

10.4.3 Glyoxal pathway

This reaction pathway, also named for a key reaction intermediate, is considerably different from all others since it involves the intermediate formation of a C—C bond. It is believed that formyl radicals (CHO·) are formed initially. The reaction sequence resembles the formaldehyde mechanism up to the formation of formic acid. However, since formic acid has a strong tendency to be oxidized rather than further reduced, Shkrob et al. [124,125] concluded that only a concerted process involving electron

transfer from the semiconductor CB to the acid coupled to a transfer of an oxygen atom from a hydroxyl group to a surface titanium atom is a feasible process for its further reaction. Formyl radicals then undergo a dimerization to glyoxal [$(CHO)_2$], which is afterwards further hydrogenated to hydroxyacetaldehyde and acetaldehyde. The splitting of acetaldehyde then yields CO and a methyl radical. The latter is then hydrogenated to yield methane. This reaction pathway does not involve methanol as intermediate or product at all, but it implies that the formation of methane is coupled to the formation of CO as by-product. Another feature of this mechanism is that it involves both reduction and oxidation steps. It is thus possible only on semiconductor powders in a photocatalytic process, and not in photoelectrochemical processes, where reduction and oxidation reactions are separated on photocathode and photoanode, respectively [2].

All mechanisms discussed above have been proposed for titanium-oxide based photocatalysts, either for crystalline TiO_2, or for isolated tetrahedral titanate species supported on or in silica. It needs to be noted that although those two photocatalysts are discussed together here, the reaction mechanism on both of them is likely very different, because TiO_2 is a semiconductor, while the isolated titanate species behaves like a molecular photocatalyst. On the other hand, an important role of four-coordinate Ti atoms also in TiO_2 has been suggested on the basis of computational results [129], so similarities might exist.

The carbene pathway is often proposed with respect to product formation on isolated titanate species. This appears reasonable, considering that only one electron-hole pair resulting from HOMO-LUMO excitation is located at each photoactive site. Accumulation of several electrons or holes for multielectron steps is thus not possible. In this respect CO has already been observed as primary single-photon, two-electron product on isolated titanate species [130]. Although formic acid, formaldehyde and methanol have frequently been reported as intermediates or products of photocatalytic CO_2 reduction on the semiconductor TiO_2 and related materials [9,63,131–136], the formaldehyde mechanism, although often proposed, is not beyond doubt. It has not been verified experimentally [2], and in a kinetic study [137] the concentration profiles of methanol and methane production did not match a consecutive formation according to the formaldehyde mechanism. In this kinetic study, the parallel formation as suggested in the carbene pathway was thus more likely [137]. In a related manner, Dey et al. [138] and Koirala et al. [139] found that methanol is preferably oxidized on TiO_2, and it was concluded that CH_4 formation did not proceed through a methanol intermediate. Both methanol and formaldehyde were found by Shkrob et al. to be primarily oxidized instead of being reduced, so after their formation they may again act as sacrificial hole scavengers [125]. Glyoxal was instead suggested as potential intermediate that is more likely to be reduced than oxidized, leading to the suggestion of the glyoxal pathway [125]. Very recently, the reactions of formic acid, formaldehyde and methanol on TiO_2 were studied under similar reaction conditions as applied in photocatalytic CO_2 reduction, but from none of these molecules, the formation of methane was observed [59]. When instead, acetic acid or acetaldehyde was offered to the photocatalyst, the formation of methane took place, and product distributions

resembled those of photocatalytic CO_2 reduction [59]. These results strongly support the glyoxal mechanism as suggested by Shkrob et al. [125]. Furthermore, acetaldehyde has also been found previously as a product of CO_2 reduction, for example using doped TiO_2 [63].

A conceptually very different mechanism for photocatalytic CO_2 reduction to CH_4 has been suggested by Look and Gafney, not for TiO_2, but for amorphous tungsten oxides on porous Vycor glass [140]. The role of the oxide in the observation of the formation of methane was explained by an *excited-state acid-base mechanism*. In this mechanism, the oxide is not a source of electrons. Instead, it shuttles electrons and holes between acidic and basic regions on its surface, where the reduction of chemisorbed CO_2 and the splitting of water can occur thermodynamically more favorably, possibly even exergonically. This hypothesis is derived based on the estimation of reaction potentials (free energies) for the reactions given in Eqs. (10.3), (10.4) as function of pH. While the former becomes more and more exergonic with higher acidity (lower pH), the latter becomes more favorable at increasingly basic pH. For reaction (10.4) to become exergonic, however, a hypothetical pH of 21 would be required. Look and Gafney suggest that the population of the WO_3 conduction band induces a charge polarization that leads to the formation of electron-deficient (acidic) and electron-rich (basic) regions in the metal oxide, where reactions (10.3), (10.4) can occur more readily. Chemisorbed CO_2, possibly in the form of formate species, is suggested to react preferably compared to physisorbed CO_2. This mechanism can also explain why amorphous WO_3 can drive CO_2 reduction, although the conduction band minimum ($+0.31 \pm 0.11$ V) is by far not negative enough to transfer a single electron onto CO_2 (-1.9 V) [140].

In summary, it cannot be conclusively decided which reaction mechanism may be in operation on the different photocatalysts, not even for the simple case of TiO_2. However, the discussion given above may be a guideline for further research on TiO_2 and other oxide materials.

10.5 Some remarks concerning photoreactors and reaction conditions

As discussed above, significant progress is still needed with respect to the development of photocatalysts and the insight into the reaction mechanism. A prerequisite to achieve these goals is the gathering of reliable data sets. This is a significant challenge, considering that the yields currently obtained in photocatalytic CO_2 reduction on virtually any photoactive material are very low. A key issue in this respect is appropriate and reliable reaction conditions. It has been shown impressively by Yang et al. [122,131] that reaction conditions of highest purity and extensive photocatalytic cleaning of the photocatalysts are required to obtain correct product yields. Similarly, Cybula et al. [60] have shown for the case of Ag-TiO_2, that hydrocarbon formation originated from contaminants in the catalyst and not from the offered $^{13}CO_2$ in the gas phase. Product formation over bare TiO_2 and other noble metal-loaded TiO_2 photocatalysts was also observed in inert

(CO_2-free) atmosphere, in spite of extensive calcination prior to the photoreaction, which is clear proof that carbon sources other than CO_2 served as reactant [60,122,131]. For Au/TiO_2/SBA-15 prepared by photodeposition in aqueous methanol solution it has been shown that the amounts of methane and ethane liberated in a cleaning experiment greatly exceeded those formed in the actual photoreaction [133]. It may be envisioned that residues from catalyst synthesis (e.g., metal-organic precursors), naturally adsorbed (bi)carbonates on oxide surfaces, or even grease from sealant materials can react photocatalytically to form "products" such as carbon monoxide, methane, methanol, or other hydrocarbons. If such processes occur, the potential of the studied material to photocatalytically convert CO_2 into useful chemicals is greatly overestimated.

There are different possibilities to assure that the detected products have actually been formed from CO_2. Ideally, the mass balance of the reaction should be solved, that is, stoichiometric amounts of methane and oxygen should be detected, ideally together with the corresponding conversion of CO_2. Since the quantification of extremely small amounts of oxygen and very small CO_2 conversions is very challenging, this ideal approach is often not feasible. Instead, a very elegant method is the use of $^{13}CO_2$ as reactant and the detection of ^{13}C-labeled products [2,60,122]. This is only possible, though, if product detection is sensitive to the molecular mass of the products, that is, by using a mass spectrometer, or if products are detected by their vibrational bands and the corresponding shift due to isotopic labeling. If other means of trace gas analysis are used, for example, a gas chromatograph with a flame-ionization detector for the detection of hydrocarbons, then the change of the carbon isotope will remain undetected. In that case, it is critical to conduct a blank experiment in which CO_2 is not fed to the reactor. It is common practice to perform blank experiments in photocatalysis, for example, a dark experiment to assure that the reaction is not thermally induced, or a reaction without catalyst to assure that it is not a pure photoreaction. However, for CO_2 reduction, it is critical to perform an experiment in which all reaction conditions are exactly the same as in the actual CO_2 reduction experiment (e.g., light intensity, amount and pretreatment of catalyst, flow rates, sealant materials), but in which the CO_2 has been exchanged by an inert gas such as helium or nitrogen. In such an experiment, products must not be detected, because they cannot be formed from CO_2 and instead must be formed from impurities. If product formation is detected, then the amounts of products detected in the actual CO_2 reduction must be corrected by the amounts detected in the blank experiment to prevent the overestimation of product formation.

Similar reaction conditions to such a blank experiment can be used for the cleaning of the photocatalyst: if a photoactive material is illuminated in the presence of water (but no CO_2) then the photogenerated charges will degrade any organic impurities present in the reacting system. Such a cleaning procedure can be carried out until no more carbon-containing products are detected or until a stable baseline is reached. When CO_2 is afterwards added to the reaction mixture with the clean photocatalyst, and an increase in product formation is detected, then this is strong evidence for product formation from CO_2 [131,133].

10.6 Examples of non-TiO_2 oxide materials for CO_2 reduction

Since the above discussion mainly concerned TiO_2, some characteristic of other classes of oxide materials in CO_2 reduction is discussed in the following. It should be noted that it is often not possible to distinguish clearly which role each of the components of a complex composite material fulfills, that is, that of a photoabsorber, that of a (co-) catalyst, or possibly that of a redox mediator. Thus, this section is ordered with respect to the materials, regardless of which function(s) they take over. Furthermore, focus is put on the product distribution and the nature of the employed material or composite. It makes little sense to compare the total yields, since the reaction conditions are usually not comparable. Such a description of material classes can never be complete, owing to already roughly 40 years of research on CO_2 reduction. Therefore, only a few examples are highlighted here that have been of particular interest in recent years.

10.6.1 Indium oxide

All studies on indium oxide for CO_2 reduction have been published very recently. In an initial report [141] of a composite of In_2O_3 and g-C_3N_4 activity tests were performed both for the hydrogen evolution in the presence of a sacrificial reagent and for the CO_2 reduction. Methane was the only hydrocarbon product reported. The three times higher yield compared to g-C_3N_4 and even four times higher yield compared to pure In_2O_3 was attributed to charge separation between the two materials, whereby the lower CB edge of In_2O_3 caused the excited electrons to end up in this material. The holes, on the other hand, ended up in the graphitic carbon nitride. The deposition of 0.5% Pt additionally doubled the methane yields [141]. On its own, In_2O_3 has mostly been studied in the hydroxylated, oxygen deficient form, $In_2O_{3-x}(OH)_y$ [142]. The reaction conditions, other than for most studies highlighted above, were those of the reverse water gas shift (RWGS) reaction, so the co-reactant was not water, but hydrogen, and expected products are carbon monoxide and water. Indeed, large amounts of CO are formed, at 150°C under light irradiation, even under simulated solar light and with just visible light (>420 nm). The material was found stable for a reaction time of 4 days. ^{13}C-labeling was employed to confirm that CO was formed from CO_2. Small amounts of CH_4 formed with and without light irradiation were instead found to originate from impurities. In this study, the activity was already traced back to the presence of surface oxygen vacancies and hydroxyl groups. In a further study [38], spectroscopic and kinetic evidence, together with computational results, provided further insight into the exact roles of those surface species. Analogously to molecular frustrated Lewis pair sites, the hydroxyls on the surface are Lewis bases, and their adjacent indium sites—next to oxygen vacancies—are Lewis acids. On those sites, hydrogen can be heterolytically split and CO_2 can be adsorbed. CO and water are then formed, whereby CO_2 dissociation is the rate-limiting step [38]. In the excited state, Lewis acidic and basic characters are enhanced, thus leading to a

lowered activation barrier under irradiation [40]. From a more practical point of view, it was found that the choice of the precursor for the $In_2O_{3-x}(OH)_y$ influenced photocatalytic activity, with indium hydroxide producing the most active photocatalysts [41]. Very recently, the defective hydroxylated indium oxide has been used for photocatalytic RWGS in a hybrid device, in which it was coated on silicon nanowires. This led to a ~6-fold increase in CO yields [43]. Alternatively, the indium oxide itself can be used in the form of nanorods [42]. Tahir et al. [35–38] instead used indium oxide as an additive to TiO_2. Both the reactions of CO_2 with water and with hydrogen were studied. In the reaction with water, doping with indium markedly increased the yield of CH_4 and longer hydrocarbons (up to C_3), while CO was the main product without indium [38]. The increased activity was attributed to improved interfacial charge transfer. Product formation was explained with a mechanism strongly resembling the carbene mechanism explained above. Rates were fitted with a Langmuir-Hinshelwood kinetic model [38]. In the reaction with hydrogen at temperatures at or above 120°C [143], selectivity switched back to CO as main product. The yield of CO was further improved by adding copper (oxide) to the photocatalyst. In this study, an additional significant increase in yields was brought about by an improved reactor design [143]. When nickel was added to In-doped TiO_2 instead of Cu, CH_4 was the main product in a reaction with water, while in a reaction with hydrogen CO was predominantly formed [36]. Again, the improved reactor design significantly increased CO yields [37]. In a very recent study, methanol was also found as by-product on Cu- and In-codoped TiO_2 [35]. When gold was added to In-TiO_2, then the photocatalyst was 99% selective for the formation of CO in the photocatalytic RWSG [144].

10.6.2 Copper oxides

The use of copper and its oxides (particularly Cu_2O) in photocatalytic CO_2 reduction is straightforward: Concerning Cu_2O as photoabsorber, it is a p-type semiconductor with a bandgap situated at negative potentials, so that electron transfer should be favorable on these materials [30,145]. Concerning the functionality as catalytic active site, metallic copper is known as classical heterogeneous catalyst for the synthesis of methanol from CO_2 in synthesis gas since the 1960s [57]. Indeed, for either CuO or Cu_2O nanorods in a composite with reduced graphene oxide (rGO), methanol was reported as main product [27]. CuO showed better performance than Cu_2O. Surprisingly, in Ref. [27] it was concluded that the rGO is responsible for the reduction reaction, not the copper oxide, since the electronic levels favor charge carrier transport in this direction. In that case, however, copper (oxide) should not act as a catalyst for the formation of methanol from CO_2, but, rather, for the oxidation reaction. In another study of Cu_2O deposited on multilayer graphene, ethanol was found as main carbon product, aside from the observation of the formation of hydrogen [28]. Reactions were carried out either in a slurry or in a capillary reactor. In this study, Cu_2O was suggested as catalytic active site, and the formation of ethanol was suggested to involve the intermediate formation of formate species [28]. Methanol was instead observed as the main product using a more complex architecture, in which

a coaxial Cu_2O nanowire array was covered with an ultrathin graphene shell onto which bimetallic Au—Cu particles were deposited [30]. It was concluded that the electrons from the Cu_2O, which functioned as photoabsorber, were transferred through the graphene layer to the Au—Cu nanoparticles which then functioned as catalytic active site for the formation of methanol. Oxygen evolution was suggested to proceed on the Cu_2O nanowires [30]. In a study with a related system of carbon-coated Cu_2O nanorods, but without additionally deposited metallic nanoparticles, CH_4 and C_2H_4 were detected as products, and carbon labeling was employed to prove the origin of those products from CO_2 [45]. In both Refs. [30,45] it was also discussed that one of the functions of the carbon coating is to prevent photocorrosion of Cu_2O, which is otherwise a severe issue. In a direct *Z*-scheme system of n-type α-Fe_2O_3 and p-type Cu_2O, on the other hand, CO was reported as predominant product [46]. In this very thorough study, the function of the two materials was clearly identified, in which the Cu_2O acted as reduction site and the Fe_2O_3 as oxidation site. Even the stoichiometric by-product oxygen was detected and quantified in Ref. [46], providing strong evidence for the formation of CO and O_2 from CO_2 in a catalytic process. Using a composite from Cu_2O and carbon quantum dots [29], methanol was the only significant product detected by GC and NMR. Here, too, Cu_2O is suggested to be the reduction site/catalyst, while the oxidation reaction is suggested to proceed on the carbon material [29]. In a composite with Cu_xO nanoparticles on strontium titanate nanotubes, it was clearly shown that the copper oxide took over the function of a cocatalyst [47]. Carbon monoxide was the main product in this study, in which the reactions were carried out in basic bicarbonate solution. Isotope labeling was used to verity that CO had been produced from CO_2, and labeling of oxygen was employed to trace the origin of gaseous oxygen back to water oxidation. It was found that the solution used for copper deposition needed to be extremely dilute, with a concentration around 0.0005 wt%, to obtain the best results [47].

10.6.3 Strontium titanate

As already outlined in the previous paragraph, a Cu_xO-$SrTiO_3$ composite led to the formation of CO as main product from the reduction of CO_2. At the same time it stoichiometrically oxidized water. In this system, $SrTiO_3$ acted as photoabsorber, and potentially as oxidation site [47]. A composite made from ZnTe and $SrTiO_3$ produced CH_4 as primary product under irradiation with visible light (≥420 nm) [146]. Although ZnTe is a p-type material, which would be beneficial for reduction reactions, the authors concluded that band alignment would favor electron transfer from this material to the $SrTiO_3$. Only ZnTe, with a bandgap of ∼2.24 eV, can be excited with visible light. In this study, $SrTiO_3$ did not act as photoabsorber itself, because it can absorb only UV light, and consequently it produced no products under irradiation with visible light. Although oxygen was not detected in Ref. [146], the authors suggested that O_2 should be produced from water oxidation at the ZnTe, because of the holes left behind in this material. To enhance visible light absorption, a study was conducted in which some of the Ti^{4+} cations were replaced by less electronegative elements, that is, Fe, Ni, and Co ions [51]. It should be noted that either Pt or RuO_2 was

additionally deposited as cocatalyst. CH_4 was the only organic product. The sample doped with Co (+Pt cocatalyst) showed the best performance, and at the same time, in comparison with the other samples, the largest amounts of CO_2 could be adsorbed on the Co-doped sample. Hydrothermal synthesis yielded better samples than solid-state synthesis [51]. Apart from $SrTiO_3$, the layered perovskite material $Sr_3Ti_2O_7$ has also been studied previously [50]. The material was additionally doped with iron, nitrogen, and/or sulfur. Methanol was found as main product, but also ethanol, acetaldehyde, ethane, and ethylene were detected in trace amounts. The sample promoted with all elements listed above (Fe, N, S) showed the highest product yields. Unfortunately, no blank experiment under the same reaction conditions, but without CO_2, was mentioned in Ref. [50], and oxygen, although it was detected, was not quantified.

10.6.4 Alkali tantalates

In a study from 2010, Teramura et al. [147] studied different $ATaO_3$ tantalates, with A = Li, Na, K. The reaction studied was not CO_2 reduction with water as coreactant, but with hydrogen. CO was found as only product. $LiTaO_3$ showed the highest activity, and it also had the largest bandgap with 4.9 eV. Thus, photocatalytic activity was found to be correlated with the optical bandgap values, that is, the wider the bandgap, the higher the CO production. Furthermore, $LiTaO_3$ chemisorbed significantly larger amounts of CO_2 than the other two tantalates [147]. In a later study [49] specifically focused on $NaTaO_3$, hydrogen was added to the $CO_2 + H_2O$ reaction mixture. Different cocatalysts were deposited on the tantalate surface. The Ru-modified sample showed highest yields of methane, while the Pt-loaded sample produced predominantly CO. Without the addition of hydrogen, the Ru-modified sample was almost inactive. In this study, it was concluded from the results of isotope labeling studies with deuterium that water is still a major source for protons in the product methane, and that hydrogen was instead needed to convert peroxide intermediates into water. With hydrogen in the reaction mixture, the Ru-modified sample showed stable productivity for 24 h, while the formation of CO on the Pt-modified sample started to decline after several hours. This was attributed to the poisoning of Pt with CO molecules [49]. In another study on $NaTaO_3$, CuO was used as cocatalyst [48]. In this study, the reaction was carried out in isopropanol, which at the same time helped to dissolve CO_2 and functioned as sacrificial reagent to trap holes. Both the formation of methanol as reduction product from CO_2 and the formation of acetone as oxidation product from isopropanol were observed. The optimal loading was determined as 2 wt % Cu. Mechanistically, it was concluded that the CuO acted as reduction site, while isopropanol oxidation occurred on the tantalate [48]. Li et al. [148] synthesized $KTaO_3$ nanoflakes in a solvent mixture of hexane and water. In a reaction system containing only CO_2 and H_2O, the nanoflakes as well as cubic reference $KTaO_3$ samples were all nearly 100% selective for the formation of CO from CO_2, with only traces of CH_4 being formed as by-product. However, large amounts of hydrogen were formed as non-carbon-containing by-product. The nanoflakes showed about an order of magnitude larger yields than conventional $KTaO_3$. The formation of oxygen was also detected in this study. The loading of silver as cocatalyst changed reaction selectivity

toward the formation of CO, while the formation of hydrogen was strongly suppressed. On the other hand, Pt as cocatalyst showed the opposite trend [148].

10.7 Concluding remarks

In this chapter, a general overview was provided of the requirements to fabricate efficient metal oxide photocatalysts for the reduction of CO_2. In this field, research can nowadays draw upon an already large pool of data, since >80% of all studies published until November 2014 have been carried out on oxide-based materials. In very recent times, carbon materials have gained increasing attention, but oxides continue to be in the focus, particularly the oxides of indium and copper, as well as titanates and tantalates. Looking at the general requirements for an active photocatalyst, the most challenging aspect clearly is the very negative LUMO energy and high thermodynamic stability of the CO_2 molecule. Other reaction pathways involving multiple electrons and protons are not situated that negative on the electrochemical energy scale, however, photoabsorbers are needed with rather negative band positions. Considering the catalytic functionality, it is questionable whether the formation of (bi)carbonates on the photocatalyst surface is beneficial, but undoubtedly the CO_2 molecule needs to be activated in some way by adsorption processes. While three major reaction pathways are discussed for TiO_2 and other photocatalyst classes, the exact pathway, in operation as function of the specific reaction conditions, is not yet clear. Reliable studies under clean conditions and with all possible blank experiments are needed, now and in the future, to shed more light on the elementary steps, if possible aided by in situ spectroscopy. Together with the knowledge on promising material classes that has already been obtained this can provide a basis to finally develop materials suitable for large-scale carbon dioxide recycling to useful chemicals.

References

[1] *https://scripps.ucsd.edu/programs/keelingcurve/*. Accessed 6 December 2016.
[2] S.N. Habisreutinger, L. Schmidt-Mende, J.K. Stolarczyk, Angew. Chem. Int. Ed. 52 (2013) 7372.
[3] L. Guo, Y. Wang, T. He, Chem. Rec. 16 (2016) 1918.
[4] H.J. Freund, M.W. Roberts, Surf. Sci. Rep. 25 (1996) 225.
[5] E.V. Kondratenko, G. Mul, J. Baltrusaitis, G.O. Larrazábal, J. Pérez-Ramirez, Energy Environ. Sci. 6 (2013) 3112.
[6] A.Y. Rozovskii, G.I. Lin, Top. Catal. 22 (2003) 137.
[7] G.C. Chinchen, P.J. Denny, D.G. Parker, M.S. Spencer, D.A. Whan, Appl. Catal. 30 (1987) 333.
[8] M. Halmann, Nature 275 (1978) 115.
[9] T. Inoue, A. Fujishima, S. Konishi, K. Honda, Nature 277 (1979) 637.
[10] Y. Zheng, L. Lin, X. Ye, F. Guo, X. Wang, Angew. Chem. Int. Ed. 53 (2014) 11926.
[11] W.-J. Ong, L.-L. Tan, S.-P. Chai, S.-T. Yong, Chem. Commun. 51 (2015) 858.
[12] W.-J. Ong, L.-L. Tan, S.-P. Chai, S.-T. Yong, A.R. Mohamed, Nano Energy 13 (2015) 757.
[13] W.-J. Ong, L.-L. Tan, S.-P. Chai, S.-T. Yong, Dalton Trans. 44 (2015) 1249.

[14] J. Qin, S. Wang, H. Ren, Y. Hou, X. Wang, Appl. Catal. B Environ. 179 (2015) 1.
[15] W. Yu, D. Xu, T. Peng, J. Mater. Chem. A 3 (2015) 19936.
[16] D. Zheng, C. Pang, X. Wang, Chem. Commun. 51 (2015) 17467.
[17] F. Raziq, Y. Qu, X. Zhang, M. Humayun, J. Wu, A. Zada, H. Yu, X. Sun, L. Jingo, J. Phys. Chem. C 120 (2016) 98.
[18] M. Li, L. Zhang, M. Wu, Y. Du, X. Fan, M. Wang, L. Zhang, Q. Kong, J. Shi, Nano Energy 19 (2016) 145.
[19] H. Shi, C. Zhang, C. Zhou, G. Chen, RSC Adv. 5 (2015) 93615.
[20] S. Yin, J. Han, T. Zhou, R. Xu, Cat. Sci. Technol. 5 (2015) 5048.
[21] S. Cao, J. Low, J. Yu, M. Jaroniec, Adv. Mater. 27 (2015) 2150.
[22] Y. He, L. Zhang, B. Teng, M. Fan, Environ. Sci. Technol. 49 (2015) 649.
[23] Y. Bai, T. Chen, P.Q. Wang, L. Wang, L. Ye, X. Shi, W. Bai, Sol. Energy Mater. Sol. Cells 157 (2016) 406.
[24] Q. Xiang, B. Cheng, J. Yu, Angew. Chem. Int. Ed. 54 (2015) 11350.
[25] K.A.S. Fernando, S. Sahu, Y. Liu, W.K. Lewis, E.A. Guliants, A. Jafariyan, P. Wang, C. E. Bunker, Y.-P. Sun, ACS Appl. Mater. Interfaces 7 (2015) 8363.
[26] J. Low, J. Yu, W. Ho, J. Phys. Chem. Lett. 6 (2015) 4244.
[27] R. Gusain, P. Kumar, O.P. Sharma, S.L. Jain, O.P. Khatri, Appl. Catal. B Environ. 181 (2016) 352.
[28] L. Hurtado, R. Natividad, H. Garcia, Catal. Commun. 84 (2016) 30.
[29] H. Li, X. Zhang, D.R. MacFarlane, Adv. Energy Mater. 5 (2015) 1401077.
[30] J. Hou, H. Cheng, O. Takeda, H. Zhu, Angew. Chem. Int. Ed. 54 (2015) 8480.
[31] L. Liu, Ceram. Int. 42 (2016) 12516.
[32] Z. Xiong, Y. Luo, Y. Zhao, J. Zhang, C. Zheng, J.C.S. Wu, Phys. Chem. Chem. Phys. 18 (2016) 13186.
[33] Y. Yang, M. Qiu, L. Liu, Ceram. Int. 42 (2016) 15081.
[34] Z. Xiong, Y. Luo, Y. Zhao, J. Zhang, C. Zheng, J.C.S. Wu, Phys. Chem. Chem. Phys. 18 (2016) 13186.
[35] M. Tahir, B. Tahir, N.A.S. Amin, H. Alias, Appl. Surf. Sci. 389 (2016) 46.
[36] M. Tahir, B. Tahir, N.A.S. Amin, A. Muhammad, Energy Convers. Manag. 119 (2016) 368.
[37] M. Tahir, N.A.S. Amin, Chem. Eng. J. 285 (2016) 635.
[38] M. Tahir, N.A.S. Amin, Appl. Catal. B Environ. 162 (2015) 98.
[39] K.K. Ghuman, T.E. Wood, L.B. Hoch, C.A. Mims, G.A. Ozin, C.V. Singh, Phys. Chem. Chem. Phys. 17 (2015) 14623.
[40] K.K. Ghuman, L.B. Hoch, P. Szymanski, J.Y.Y. Loh, N.P. Kherani, M.A. El-Sayed, G. A. Ozin, C.V. Singh, J. Am. Chem. Soc. 138 (2016) 1206.
[41] L.B. Hoch, L. He, Q. Qiao, K. Liao, L.W. Reyes, Y. Zhu, G.A. Ozin, Chem. Mater. 28 (2016) 4160.
[42] L. He, T.E. Wood, B. Wu, Y. Dong, L.B. Hoch, L.M. Reyes, D. Wang, C. Kübel, C. Qian, J. Jia, K. Liao, P.G. O'Brien, A. Sandhel, J.Y.Y. Loh, P. Szymanski, N.P. Kherani, T. C. Sum, C.A. Mims, G.A. Ozin, ACS Nano 10 (2016) 5578.
[43] L.B. Hoch, P.G. O'Brien, A. Jelle, A. Sandhel, D.D. Perovic, C.A. Mims, G.A. Ozin, ACS Nano 10 (2016) 9017.
[44] S. Zhu, S. Liang, Y. Tong, X. An, J. Long, X. Fu, X. Wang, Phys. Chem. Chem. Phys. 17 (2015) 9761.
[45] L. Yu, G. Li, X. Zhang, X. Ba, G. Shi, Y. Li, P.K. Wong, J.C. Yu, Y. Yu, ACS Catal. 6 (2016) 6444.

[46] J.-C. Wang, L. Zhang, W.-X. Fang, J. Ren, Y.-Y. Li, H.-C. Yao, J.-S. Wang, Z.-J. Li, ACS Appl. Mater. Interfaces 7 (2015) 8631.
[47] S. Shoji, G. Yin, M. Nishikawa, D. Atarashi, E. Sakai, M. Miyauchi, Chem. Phys. Lett. 658 (2016) 309.
[48] T. Xiang, F. Xin, J. Chen, Y. Wang, X. Yin, X. Shao, Beilstein J. Nanotechnol. 7 (2016) 776.
[49] M. Li, P. Li, K. Chang, T. Wang, L. Liu, Q. Kang, S. Ouyang, J. Ye, Chem. Commun. 51 (2015) 7645.
[50] V. Jeyalakshmi, R. Mahalakshmy, K. Ramesh, P.V.C. Rao, N.V. Choudary, G.S. Ganesh, K. Thirunavukkarasu, K.R. Krishnamurthy, B. Viswanathan, RSC Adv. 5 (2015) 5958.
[51] J. Kou, J. Gao, Z. Li, H. Yu, Y. Zhou, Z. Zou, Catal. Lett. 145 (2015) 640.
[52] Y. Zhao, X. Jia, G.I.N. Waterhouse, L.-Z. Wu, C.-H. Tung, D. O'Hare, T. Zhang, Adv. Energy Mater. 6 (2016) 1501974.
[53] H. Zhao, J. Xu, L. Liu, G. Rao, C. Zhao, Y. Li, J. CO_2 Util. 15 (2016) 15.
[54] S. Iguchi, K. Teramura, S. Hosokawa, T. Tanaka, Appl. Catal. A Gen. 521 (2016) 160.
[55] M. Lv, H. Liu, J. Solid State Chem. 227 (2015) 232.
[56] C. Zhao, L. Liu, G. Rao, H. Zhao, L. Wang, J. Xu, Y. Li, Cat. Sci. Technol. 5 (2015) 3288.
[57] D. Saliba, A. Ezzeddine, R. Sougrat, N.M. Khashab, M. Hmadeh, M. Al-Ghoul, ChemSusChem 9 (2016) 800.
[58] Q. Guo, Q. Zhang, H. Wang, Z. Liu, Z. Zhao, Catal. Commun. 77 (2016) 118.
[59] A. Pougin, M. Dilla, J. Strunk, Phys. Chem. Chem. Phys. 18 (2016) 10809.
[60] A. Cybula, M. Klein, A. Zaleska, Appl. Catal. B Environ. 164 (2015) 433.
[61] K.-Y. Lee, K. Sato, A.R. Mohamed, Mater. Lett. 163 (2016) 240.
[62] J.-H. Lee, H. Lee, M. Kang, Mater. Lett. 178 (2016) 316.
[63] O. Ola, M.M. Maroto-Valer, Appl. Catal. A Gen. 502 (2015) 114.
[64] H. Park, H.-H. Ou, U. Kang, J. Choi, M. Hoffmann, Catal. Today 266 (2016) 153.
[65] X. Xin, T. Xu, L. Wang, C. Wang, Sci. Rep. 6 (2016) 23684.
[66] Z. He, J. Tang, J. Shen, J. Chen, S. Song, Appl. Surf. Sci. 364 (2016) 416.
[67] W. Qingli, Z. Zhaoguo, C. Xudong, H. Zhengfeng, D. Peimei, C. Yi, Z. Xiwen, J. CO2 Util. 12 (2015) 7.
[68] Y. Wang, J. Jiao, Z. Zhao, J. Liu, J. Li, G. Jiang, Y. Wang, A. Duan, Appl. Catal. B Environ. 179 (2015) 422.
[69] Y. Cao, Q. Li, C. Li, J. Li, J. Yang, Appl. Catal. B Environ. 198 (2016) 378.
[70] M.S. Akple, J. Low, Z. Qin, S. Wageh, A.A. Al-Ghamdi, J. Yu, S. Liu, Chin. J. Catal. 36 (2015) 2127.
[71] S. Qamar, F. Lei, L. Liang, S. Gao, K. Liu, Y. Sun, W. Ni, Y. Xie, Nano Energy 26 (2016) 692.
[72] P. Reñones, A. Moya, F. Fresno, L. Collado, J.J. Vilatela, V.A. de la Peña O'Shea, J. CO_2 Util. 15 (2016) 24.
[73] L. Yuan, C. Han, M. Pagliaro, Y.-J. Xu, J. Phys. Chem. C 120 (2016) 265.
[74] E. Korovin, D. Selishchev, D. Kozlov, Top. Catal. 59 (2016) 1292.
[75] H. Park, H.-H. Ou, A.J. Colussi, M.R. Hoffmann, J. Phys. Chem. A 119 (2015) 4658.
[76] A.L. Linsebigler, G. Lu, J.T. Yates, Chem. Rev. 95 (1995) 735.
[77] J. Schneider, M. Matsuoka, M. Takeuchi, J. Zhang, Y. Horiuchi, M. Anpo, D. W. Bahnemann, Chem. Rev. 114 (2014) 9919.
[78] R. van de Krol, Principles of photoelectrochemical cells, in: R. van de Krol, M. Grätzel (Eds.), Photoelectrochemical Hydrogen Production, Springer Series Electronic Materials: Science & Technology, Springer Science-Business Media, New York, 2012.

[79] J. Nowotny, Oxide Semiconductors for Solar Energy Conversion–Titanium Dioxide, CRC Press, Taylor and Francis, Boca Raton, FL, 2012.
[80] M.A. Henderson, Surf. Sci. Rep. 66 (2011) 185.
[81] A. Fujishima, X. Zhang, D.A. Tryk, Surf. Sci. Rep. 63 (2008) 515.
[82] P.W. Atkins, Physical Chemistry, 5th ed., Oxford University Press, Melbourne, Tokyo, 1994.
[83] D.P. Colombo, R.M. Bowman, J. Phys. Chem. 100 (1996) 18445.
[84] R. Beránek, Adv. Phys. Chem. (2011) 786759.
[85] J. Li, N. Wu, Cat. Sci. Technol. 5 (2015) 1360.
[86] J. Zhang, P. Zhou, J. Liu, J. Yu, Phys. Chem. Chem. Phys. 16 (2014) 20382.
[87] S. Buller, J. Strunk, J. Energy Chem. 25 (2016) 171.
[88] O. Carp, C.L. Huismann, A. Reller, Prog. Solid State Chem. 32 (2004) 33.
[89] M. Matsuoka, M. Anpo, Local structures, excited states, and photocatalytic reactivities of "single-site" Ti-oxide photocatalysts constructed within zeolites or mesoporous materials, in: M. Anpo, P.V. Kamat (Eds.), Environmentally Benign Photocatalysts: Applications of Titanium Oxide Based Materials, Springer Science-Business Media, New York, 2010.
[90] D.W. Bahnemann, C. Kormann, M.R. Hoffmann, J. Phys. Chem. 91 (1987) 3789.
[91] J.A. Anta, Curr. Opin. Colloid Interface Sci. 17 (2012) 124.
[92] F.-X. Xiao, J. Miao, H.B. Tao, S.-F. Hung, H.-Y. Wang, H.B. Yang, J. Chen, R. Chen, B. Liu, Small 11 (2015) 2115.
[93] H.-M. Xu, H.-C. Wang, Y. Shen, Y.-H. Lin, C.-W. Nan, J. Adv. Ceram. 4 (2015) 159.
[94] J.S. Lee, J. Jang, J. Ind. Eng. Chem. 20 (2014) 363.
[95] J. Tian, Z. Zhao, A. Kumar, R.I. Boughton, H. Liu, Chem. Soc. Rev. 43 (2014) 6920.
[96] B. Weng, S. Liu, Z.-R. Tang, Y.-J. Xu, RSC Adv. 4 (2014) 12685.
[97] F.E. Osterloh, Chem. Soc. Rev. 42 (2013) 2294.
[98] B. Levy, J. Electroceram. 1:3 (1997) 239.
[99] D. Chen, X. Zhang, A.F. Lee, J. Mater. Chem. A 3 (2015) 14487.
[100] H. Wilmer, M. Kurtz, K.V. Klementiev, O.P. Tkachenko, W. Grünert, O. Hinrichsen, A. Birkner, S. Rabe, K. Merz, M. Driess, C. Wöll, M. Muhler, Phys. Chem. Chem. Phys. 5 (2003) 4736.
[101] M. Kurtz, J. Strunk, O. Hinrichsen, M. Muhler, K. Fink, B. Meyer, C. Wöll, Angew. Chem. Int. Ed. 44 (2005) 2790.
[102] S. Polarz, J. Strunk, V. Ischenko, M.W.E. van den Berg, O. Hinrichsen, M. Muhler, M. Driess, Angew. Chem. Int. Ed. 45 (2006) 2965.
[103] T. Mclaren, G. Valdes-Solis, S.C. Li, J. Tsang, Am. Chem. Soc. 131 (2009) 12540.
[104] A.T. Goodrow, J. Bell, Phys. Chem. C 112 (2008) 13204.
[105] P.L.D. Lindan, N.M. Harrison, M.J. Gillan, J.A. White, Phys. Rev. B 55 (1997) 15919.
[106] A.T. Paxton, L. Thiên-Nga, Phys. Rev. B 57 (1998) 1579.
[107] V. Ischenko, S. Polarz, D. Grote, V. Stavarache, K. Fink, M. Driess, Adv. Funct. Mater. 15 (2005) 1945.
[108] A. Janotti, C.G. Van de Walle, Rep. Prog. Phys. 72 (2009) 126501.
[109] L. Liu, H. Zhao, J.M. Andino, Y. Li, ACS Catal. 2 (2012) 1817.
[110] L. Liu, F. Gao, H. Zhao, Y. Li, Appl. Catal. B Environ. 134–135 (2013) 349.
[111] V.P. Indrakanti, H.H. Schobert, J.D. Kubicki, Energy Fuel 23 (2009) 5247.
[112] W. Tu, Y. Zhou, Z. Zou, Adv. Mater. 26 (2014) 4607.
[113] B. Ohtani, J Photochem. Photobiol. C: Photochem. Rev. 11 (2010) 157.
[114] K. Iizuka, T. Wato, Y. Miseki, K. Saito, A. Kodu, J. Am. Chem. Soc. 133 (2011) 20863.

[115] K. Teramura, S. Iguchi, Y. Mizuno, T. Shishido, T. Tanaka, Angew. Chem. Int. Ed. 51 (2012) 8008.
[116] D. Uner, M.M. Oymak, Catal. Today 181 (2012) 82.
[117] S. Ristig, N. Cibura, J. Strunk, Green 5 (2015) 23.
[118] M.S. Hamdy, R. Amrollahi, I. Sinev, B. Mei, G. Mul, J. Am. Chem. Soc. 136 (2014) 594.
[119] M. Marszewski, S. Cao, J. Yu, M. Jaroniec, Mater. Horiz. 2 (2015) 261.
[120] G. Busca, V. Lorenzelli, Mater. Chem. 7 (1982) 89.
[121] Y. Wang, R. Kováčik, B. Meyer, K. Kotsis, D. Stodt, V. Staemmler, H. Qiu, F. Traeger, D. Langenberg, M. Muhler, C. Wöll, Angew. Chem. Int. Ed. 46 (2007) 5624.
[122] C.C. Yang, Y.H. Yu, B. van der Linden, J.C.S. Wu, G. Mul, J. Am. Chem. Soc. 132 (2010) 8398–8406.
[123] N.M. Dimitrijevic, B.K. Vijayan, O.G. Poluektov, T. Rajh, K.A. Gray, H.Y. He, P. Zapol, J. Am. Chem. Soc. 133 (2011) 3964.
[124] I.A. Shkrob, N.M. Dimitrijevic, T.W. Marin, H. He, P. Zapol, J. Phys. Chem. C 116 (2012) 9461.
[125] I.A. Shkrob, T.W. Marin, H. He, P. Zapol, J. Phys. Chem. C 116 (2012) 9450.
[126] C. Liu, H. He, P. Zapol, L.A. Curtiss, Phys. Chem. Chem. Phys. 16 (2014) 26584.
[127] M. Anpo, K. Chiba, J. Mol. Catal. 74 (1992) 207.
[128] M. Anpo, H. Yamashita, Y. Ichihashi, S. Ehara, J. Electroanal. Chem. 396 (1995) 21.
[129] D. Lee, Y. Kanai, J. Am. Chem. Soc. 134 (2012) 20266.
[130] W. Lin, H. Han, H. Frei, J. Phys. Chem. B 108 (2004) 18269.
[131] M. Halmann, M. Ulman, B. Aurian-Blajeni, Sol. Energy 31 (1983) 429.
[132] C.C. Yang, J. Vernimmen, V. Meynen, P. Cool, G. Mul, J. Catal. 284 (2011) 1.
[133] B. Mei, A. Pougin, J. Strunk, J. Catal. 306 (2013) 184.
[134] K. Kočí, K. Matějů, L. Obalová, S. Krejčíková, Z. Lacný, D. Plachá, L. Čapek, A. Hospodková, O. Šolcová, Appl. Catal. B Environ. 96 (2010) 239.
[135] J.C.S. Wu, H.-M. Lin, Int. J. Photoenergy 7 (2005) 115.
[136] G.R. Dey, J. Nat. Gas Chem. 16 (2007) 217.
[137] L. Kočí, O.Š. Obalová, Chem. Process. Eng. 31 (2010) 395.
[138] G.R. Dey, A.D. Belapurkar, K. Kishore, J. Photochem. Photobiol. A Chem. 163 (2004) 503.
[139] R. Koirala, S. Docao, S.B. Lee, K.B. Yoon, Catal. Today 243 (2015) 235.
[140] J.C.S. Wu, H.-M. Lin, Int. J. Photoenergy 7 (2005) 115.
[141] S.-W. Cao, X.-F. Liu, Y.-P. Yuan, Z.-Y. Zhang, Y.-S. Liao, J. Fang, S.C.J. Loo, T. C. Sum, C. Xue, Appl. Catal. B Environ. 147 (2014) 940.
[142] L.B. Hoch, T.E. Wood, P.G. O'Brien, K. Liao, L.M. Reyes, C.A. Mims, G.A. Ozin, Adv. Sci. 1 (2014) 1400013.
[143] M. Tahir, N.A.S. Amin, Appl. Catal. A Gen. 493 (2015) 90.
[144] B. Tahir, M. Tahir, N.A.S. Amin, Appl. Surf. Sci. 338 (2015) 1.
[145] A. Paracchino, V. Laporte, K. Sivula, M. Grätzel, E. Thimsen, Nat. Mater. 10 (2011) 456.
[146] M.F. Ehsan, M.N. Ashiq, F. Bi, Y. Bi, S. Palanisamy, T. He, RSC Adv. 4 (2014) 48411.
[147] K. Teramura, S. Okuoka, H. Tsuneoka, T. Shishido, T. Tanaka, Appl. Catal. B Environ. 96 (2010) 565.
[148] K. Li, A.D. Handoko, M. Khraisheh, J. Tang, Nanoscale 6 (2014) 9767.